Journal of Nuclear Medicine, published on December 31, 2014 as doi:10.2967/jnumed.114.147744

Integrated ^{18}F-FDG-PET/MRI in the assessment of cardiac masses: A pilot study.

Felix Nensa[1], Ercan Tezgah[2], Thorsten D. Poeppel[3], Christoph J. Jensen[4], Juliane Schelhorn[1], Jens Köhler[5], Philipp Heusch[6], Oliver Bruder[4], Thomas Schlosser[1], Kai Nassenstein[1]

[1] Department of Diagnostic and Interventional Radiology and Neuroradiology, University Hospital Essen, University of Duisburg-Essen, Essen, Germany

[2] Clinic for Cardiology, University Hospital Essen, University of Duisburg-Essen, Essen, Germany

[3] Clinic for Nuclear Medicine, University Hospital Essen, University of Duisburg-Essen, Essen, Germany

[4] Department of Cardiology and Angiology, Contilia Heart and Vascular Center, Elisabeth Hospital Essen, Essen, Germany

[5] Department of Medicine (Cancer Research), West German Tumor Center, University Hospital of University Duisburg-Essen, Essen, Germany

[6] Department of Diagnostic and Interventional Radiology, University Hospital Dusseldorf, University of Dusseldorf, Dusseldorf, Germany

Corresponding author

Felix Nensa, MD

University Hospital Essen

Department of Diagnostic and Interventional Radiology and Neuroradiology

Hufelandstrasse 55, Essen, Germany

Email: felix.nensa@uk-essen.de

Phone: +49 (0)201 / 723-1501

Fax: +49 (0)201 / 723-1548

Word count: 4711

Running title: ^{18}F-FDG-PET/MRI in cardiac masses

ABSTRACT

The objective of the present study was to evaluate whether integrated ^{18}F-FDG-PET/MRI can improve the diagnostic workup in patients with cardiac masses.

Methods: Twenty patients were prospectively assessed using integrated cardiac ^{18}F-FDG-PET/MRI: 16 patients with cardiac masses of unknown identity and four patients with cardiac sarcoma after surgical therapy. All scans were performed on an integrated 3-T PET/MR device (mMR Biograph, Siemens Healthcare, Erlangen, Germany). The MR protocol consisted of HASTE, cine and T2-weighted images as well as T1-weighted images before and after injection of gadobutrol. PET data acquisition was performed simultaneously to the MR scan after injection of 199±58 MBq ^{18}F-FDG. Patients were prepared with a high-fat, low-carbohydrate diet in a period of 24 hours before the examination and 50 IU/kg of unfractionated heparin were administered intravenously 15 minutes prior the ^{18}F-FDG injection.

Results: Cardiac masses were diagnosed as follows: 3 x metastases, 1 x direct tumor infiltration via pulmonary vein, 2 x local relapse of primary sarcoma after surgery, 1 Burkitt's lymphoma, 2 x scar/patch tissue after surgery of primary sarcoma, 4 x myxoma, 1 x fibroelastoma, 3 x caseous calcification of mitral annulus (CCMA), 3 x thrombus. SUV_{max} in malignant lesions was significantly higher than in non-malignant cases (13.2±6.2 vs. 2.3±1.2, p=0.0004). Using a threshold of ≥ 5.2, SUV_{max} was found to yield 100% sensitivity and 92% specificity for the differentiation between malignant and non-malignant cases. T2-weighted hyperintensity and contrast-enhancement both yielded 100% sensitivity, but a weak specificity of 54% and 46%, respectively. Morphologic tumor features as assessed by cine MRI yielded 86% sensitivity and 92% specificity.

Consent reading using all available MR features yielded 100% sensitivity and 92% specificity. A Boolean 'AND' combination of SUV_{max} ≥ 5.2 with consent MRI reading improved sensitivity and specificity to 100%.

Conclusion: In selected patients, ^{18}F-FDG-PET/MRI can improve the noninvasive diagnosis and follow-up of cardiac masses.

Keywords: PET/MRI; ^{18}F-FDG; cardiac tumor; cardiac malignancy

INTRODUCTION

Cardiac tumors are rare. Primary cardiac tumors have been found in autopsy at an incidence of about 0.02% (*1*). About 75% of primary tumors are benign and 25% malignant (*1*). In contrast, secondary cardiac tumors (e.g. metastases) are found in more than 10% of tumor patients at autopsy. The most frequent primary cardiac tumors are atrial myxoma in adults and rhabdomyosarcoma in children (*1, 2*). However, cardiac thrombus is the most frequent intracavitary mass. In some instances, this can be challenging to differentiate from a cardiac neoplasm using conventional echocardiographic assessment methods. (*3*).

Due to resulting cardiac functional cardiac disorders the treatment of choice in most tumor cases is complete resection. Furthermore, in malignant tumors surgery will be combined with chemo- and/or radiotherapy. For preoperative planning, assessment of tumor malignancy, expansion and its relation to critical structures like valves or papillary muscles by imaging is often critical. Also, post-treatment identification of local relapse by imaging is an important element of the overall treatment strategy.

Cross sectional imaging like CT, MRI or echocardiography in many cases provides excellent depiction of tumor morphology, that may allow for the assessment of malignancy or may even predict histological diagnosis (*4-8*). Cardiac MRI (CMR) has been shown to be particularly helpful in the diagnostic workup of cardiac tumors (*4,9*). More recently ^{18}F-FDG PET/CT has been shown, to provide incremental diagnostic information in the determination of malignancy and staging of cardiac tumors (*10*).

Integrated ^{18}F-FDG PET/MRI provides a combination of superior morphologic tumor characterization and visualization of tumor metabolism (*11-14*) and thus, might hold great potential in the diagnosis and follow-up of cardiac tumors.

In this pilot study, we sought to evaluate if integrated ^{18}F-FDG PET/MRI provides significant benefit over ^{18}F-FDG PET or MRI alone.

MATERIALS AND METHODS

Patients

Twenty patients were prospectively enrolled in this study: 16 patients suffered from cardiac masses of unknown identity (n=12 found by echocardiography; n=4 found by CT) and four patients presented with cardiac sarcoma after surgical therapy.

Patient entry criteria included: age of ≥18 years; cardiac mass of unknown identity or indication for follow-up imaging after resection of cardiac malignancy; no contraindications against the application of gadolinium-based contrast agents or general MR imaging contraindications. Two patients were excluded from the analysis: One patient with echocardiographically detected intracavitary mass in the right atrium was excluded due to incomplete PET/MR examination caused by claustrophobia. One patient with angiographically seen focal contrast-enhancement of the septal wall was excluded, because the suspected tumor was not found in PET/MRI and thus considered an artifact.

All patients underwent simultaneous cardiac PET/MRI and were prepared with a customized study information sheet and informed consent discussion. The present study was approved by the local institutional review board. All patients gave written informed consent prior to their examination.

Scanner

All scans were performed on an integrated whole-body PET/MRI system with 3 Tesla field strength (Biograph mMR, Siemens Healthcare, Erlangen, Germany) coupled to lutetium oxyorthosilicate (LSO) avalanche photodiodes (APD) for PET-acquisition (*15*).

PET Protocol

To suppress physiological glucose uptake in the myocardium, the patients were prepared with a high-fat, low-carbohydrate diet in a period of 24 hours before the examination and 50 IU/kg of unfractionated heparin were intravenously administered 15 minutes before the ^{18}F-FDG injection. Blood glucose levels at the time of tracer injection were < 120 mg/dl.

An activity of 199±58 MBq ^{18}F-FDG was administered intravenously. The PET/MR scan started 94±35 min after injection of ^{18}F-FDG and comprised a cardiac PET-scan with 1 bed position (61±7 min) and 3D image reconstruction (2x2x2 mm voxel size) using ordinary Poisson ordered-subset expectation maximization (OP-OSEM) with 3 iterations and 21 subsets, a Gaussian filter with 5.0 mm full-width at half-maximum (FWHM) and a 344x344 image matrix. For automatic attenuation correction of the acquired PET data a four-compartment-model attenuation map was calculated from fat-only and water-only Dixon-based sequences by segmentation into background, lung, fat and soft tissue (*16*).

MRI Protocol

All examinations were performed including the following sequences. First, an axial 2D half Fourier acquisition single shot turbo spin echo sequence was performed (HASTE; TR: 510 - 938 ms; TE: 51 ms; slice thickness: 8 mm; matrix size: 256 × 105; in-plane resolution: 1.0♯× 2.3 mm to 1.0♯× 2.5 mm [depending on patient body habitus]). Then, balanced steady-state free precession sequences (Cine; TR: 3.44 ms; TE: 1.51 ms; slice thickness: 8 mm; matrix size: 216 × 256; in-plane resolution: 0.9♯× 1.7 mm to 0.9♯× 2.0 mm [depending on patient body habitus]) were performed. This was followed by 2D

turbo spin echo T1-weighted sequences (T1w;TR: one R-R interval; TE: 27 ms ; echo train length: 9; flip angle: 180°; slice thickness: 5 mm; matrix size: 256 × 208; in-plane resolution: 0.8# 2.1 mm to 1.1# 1.6 mm [depending on patient body habitus]). Then, 2D turbo-inversion recovery-magnitude T2-weighted sequences with short inversion time were performed (T2w; TI: 180 ms; TR: two R-R intervals; TE: 44 ms; echo train length: 20; flip angle: 180°; slice thickness: 8 mm; matrix size: 256 × 130; in-plane resolution: 1.0 × 1.7 mm to 0.9 × 1.9 mm [depending on patient body habitus]). Finally, 2D turbo spin echo T1-weighted post-contrast sequences with spectral fat saturation were performed (pcT1w; TR: one R-R interval; TE: 27 ms; echo train length: 9; flip angle: 180°; slice thickness: 5 mm; matrix size: 208 × 256; in-plane resolution: 0.5 × 1.1 mm to 1.1 × 1.6 mm [depending on patient body habitus])

All sequences were ECG-triggered and acquired in breath-hold. The mean heart rate was 75 [47 to 102] beats per minute, corresponding to a mean R-R interval of 840 [587 to 1289] ms. HASTE images were acquired in axial slices covering the whole thorax. Cine images were acquired in 4-, 3- and 2-chamber views (4CV, 3CV, 2CV) and in contiguous short-axis views (SA) covering the entire heart. T1w, T2w and pcT1w images were acquired in two orthogonal slices both cross-secting the tumor. Before the acquisition of pcT1w images Gadobutrol (Gadovist®, Bayer Healthcare, Leverkusen, Germany) was administered as contrast agent at a weight-adapted dosage of 0.1 mmol/kg body weight. Patients were scanned supine with their arms at their sides (arm-down position).

Image Analysis

Tumor characteristics were analyzed by two readers in consensus (both board-certified radiologists with > 10 years of experience in cardiac MRI and oncologic PET). Volumetric assessment of tumor size was performed manually in HASTE images using OsiriX imaging software (OsiriX Foundation, Geneva, Switzerland). Signal intensity of the tumors in T1w and T2w images as well as contrast-enhancement in pcT1w images were visually classified with reference to the normal myocardium. Pericardial effusion was assessed in cine SSFP images.

Morphologic tumor characteristics were assessed using cine SSFP images. Findings were classified according to characteristic features as being rather malignant or rather benign. Malignant classification comprised close attachment to adjacent tissue and/or infiltration, extracardiac extension, irregular tumor margin and inhomogeneity in signal intensity. Benign classification comprised intracavitary location, blood flow dependent mobility, rounded shape and homogeneous signal intensity. If characteristic features for malignancy and benignancy were present within one lesion, features were weighted based on their explicitness by both readers in consensus.

Mean standardized uptake values (SUV) of the blood pool were measured using 3-dimensional volumes of interest (VOI) placed in the left ventricular cavity, not including any papillary muscles. Maximum SUVs (SUV_{max}) were measured using VOIs fully encompassing the tumors.

Statistical Analysis

Variables were given as arithmetic mean ± standard deviation unless otherwise specified. Group comparisons were performed using Wilcoxon and Chi^2 tests as appropriate. Correlation analyses were performed using the Spearman rank correlation

coefficient. Classification analysis was performed using receiver-operating-characteristics. Significance was inferred at a level of $p < 0.05$. All statistical calculations were performed using the R-software environment for statistical computing (R Foundation for Statistical Computing, Vienna, Austria).

RESULTS

Cardiac masses were diagnosed as follows (Table 1): 3 x metastases (Fig. 1), 1 x direct infiltration via pulmonary vein, 2 x local relapse of primary sarcoma after surgery (Fig. 2), 1 Burkitt's lymphoma, 2 x scar/patch tissue after surgery of primary sarcoma, 4 x myxoma (Fig. 3), 1 x fibroelastoma, 3 x caseous calcification of mitral annulus (CCMA; Fig. 4), 3 x thrombus (Fig. 1). Diagnosis was histologically proven in 15 patients. In 3 patients with CCMA no biopsy was acquired, because typical location and calcifications (found in additional CT scans) were considered sufficient for diagnosis and surgery was not indicated. In two patients with scar/patch tissue after surgery, diagnosis was confirmed via follow-up MR scans.

In three patients additional metastases have been detected by PET/MRI. In one patient with local relapse of cardiac angiosarcoma, additional pulmonary metastases were found (Table 1, No. 6). In one patient with no local relapse after resection of cardiac fibrosarcoma, a metastasis in the upper right thoracic wall was found (Table 1, No. 9). In one patient with anal carcinoma and a large thrombus in the right ventricular outflow tract, mediastinal lymph node metastases were found (Table 1, No. 18; Fig. 1).

FDG Uptake

The mean SUV in the blood pool was 1.3±0.3 (range: 0.8 to 2.1; n = 20). The mean SUV_{max} in primary and secondary malignant tumors was 13.2±6.2 (range: 5.2 to 21.3; n = 7). The mean SUV_{max} in benign tumors and thrombi was 2.0±0.9 (range: 1.0 to 3.8; n = 11). The mean SUV_{max} in all non-malignant cases (benign tumors, thrombi and scar tissue) was 2.3±1.2 (range: 1.0 to 5.2; n = 13). The mean SUV_{max} was significantly

higher in malignant tumors (Wilcoxon test p = 0.0004).

Malignant and benign cases overlapped at an SUV_{max} of 5.2, that was found in one patient with cardiac metastases of angiosarcoma of the limb (Table 1, No. 3) and in another patient with patch tissue after resection of a primary fibrosarcoma (Table 1, No. 9).

A statistically significant correlation between tumor size and SUV_{max} was found (Spearman rho = 0.60, p = 0.005).

MRI

Mean tumor volume was significantly larger in malignant cases (140±171 ml vs. 17±23 ml, Wilcoxon test p = 0.0012). Pericardial effusion was found in five out of seven malignant-cases and in two out of 13 non-malignant cases (Chi^2 test p = 0.044). All malignant cases showed hyperintense signal in T2-weighted images. However, T2w hyperintensity was also found in six out of 13 non-malignant cases (Chi^2 test p = 0.055). All malignant cases showed contrast-enhancement in T1-weighted images after i.v. injection of a gadolinium-based contrast agent. However, contrast-enhancement was also found in seven out of 13 non-malignant cases (Chi^2 test p = 0.102). Six out of seven malignancies were correctly identified by morphologic features using cine SSFP imaging, while 12 out of 13 non-malignant cases were correctly identified (Chi^2 test p = 0.003). Considering all available MR features, consent reading correctly identified all seven malignancies, while also one non-malignant case was falsely classified as being malignant (Chi^2 test p = 0.0004).

Classification Analysis

Receiver-operating-characteristic analysis showed SUV_{max} to identify malignant cases best when using a threshold of ≥ 5.2, resulting in 100% sensitivity and 92% specificity. Tumor volume was found to identify malignant cases best when using a threshold of ≥ 23.1 ml, resulting in 100% sensitivity and 85% specificity. T2-weighted hyperintensity and contrast-enhancement both yielded 100% sensitivity, but a weak specificity of 54% and 46%, respectively. Pericardial effusion yielded 71% sensitivity and 85% specificity. Morphologic tumor features as assessed by cine MRI yielded 86% sensitivity and 92% specificity. Consent reading using all available MR features yielded 100% sensitivity and 92% specificity. A Boolean 'AND' combination of SUV_{max} ≥ 5.2 with consent MRI reading improved sensitivity and specificity to 100% (Table 2).

DISCUSSION

In this study we sought to evaluate whether integrated ^{18}F-FDG PET/MRI can improve the diagnostic workup of cardiac tumors. Interpreted independently, we found both ^{18}F-FDG PET and MRI to yield 100% sensitivity and 92% specificity in determining tumor malignancy. A combination of ^{18}F-FDG PET and MRI yielded 100% sensitivity and specificity, when both tests were required to be positive for diagnosing malignancy. Perfect classification (100% sensitivity and specificity) is extremely unlikely for any biomedical test. However, one has to consider that first, as well ^{18}F-FDG PET as cardiac MRI alone have already been reported to yield high sensitivity and specificity (*9,10*), and secondly, the sample size in the present study was relatively small. In fact, there were just two cases (both with an SUV_{max} of 5.2) that could not be differentiated using ^{18}F-FDG PET alone. Classification by any "optimal" SUV_{max} threshold would correctly classify one and misclassify the other, resulting in only one misclassification in 20 cases. Thus, any more sensible values for sensitivity and specificity (e.g. > 95%, but < 100%) could not be expected due to the small sample size. Considering both ^{18}F-FDG PET and MRI, these findings could be unequivocally identified as malignancy in the one case and patch tissue in the other. In another case, where scar tissue was misclassified by MRI as local relapse of cardiac angiosarcoma, a relatively low SUV_{max} of 2.2 made malignant relapse very unlikely. Therefore, these findings indicate additional value of PET/MRI in selected cases.

An ^{18}F-FDG PET/CT study by Rahbar et al. in 24 patients with cardiac tumors yielded 100% sensitivity with 86% specificity at an SUV_{max} cutoff of 3.5 and 94% sensitivity with

100% specificity at an SUV_{max} cutoff of 4.6 (*10*), which was similar to our findings. In fact, applying their cutoff of 3.5 to our data yielded nearly the same values for sensitivity (100%) and specificity (85%). T1-weighted and contrast-enhanced MRI were found to yield high sensitivity but low specificity which was expected from known MR characteristics of cardiac tumors (*4,17,18*). Hyperintensity on native T1-weighted images was not helpful as a classifier on its own, but is a prerequisite to reliably evaluate contrast-enhancement on T1-weighted post-contrast images. Because size and metabolism are predictors of tumor malignancy, a certain correlation between both was anticipated. Interestingly such a correlation was not found in the study by Rahbar et al., which might be explained by their one-dimensional assessment of tumor size (*10*).

As clinical availability of integrated PET/MRI rises (*14*) and the feasibility of cardiac PET/MRI has been demonstrated (*19*), it is important to know, whether ^{18}F-FDG PET/MRI provides added value over established imaging methods in the assessment of cardiac tumors. ^{18}F-FDG PET/CT alone can quite accurately discriminate between malignant and benign tumors, however, CT is suboptimal for the pre-surgical assessment of tumor morphology. Cardiac MRI allows for excellent delineation of cardiac tumors due to high soft tissue contrast, particularly regarding infiltration in adjacent tissue and the involvement of critical structures such as valves or papillary muscles. Also impairment of cardiac function can be measured by quantification of systolic function, wall motion and blood flow. Integrated ^{18}F-FDG PET/MRI obviously combines the advantages of both methods within a single examination and moreover seems to be the most accurate method for the determination of malignancy. However, in many cases sequential PET/CT and MRI (with or without post-hoc fusion) might be equally well suited, with the exception of those cases were optimal co-registration is

essential. Particularly the differentiation of scar tissue vs. relapse in follow-up examinations after surgery of cardiac malignancies might benefit from simultaneous PET/MRI.

The main limitation of this study is the small sample size. Cardiac tumors are rare and integrated PET/MRI has been available just for a few years. Thus, the results of this pilot study must be considered preliminary and further multicenter studies and meta-analyses should follow. Another limitation was the availability of a histological reference standard in only 15 of 20 patients. However, in all five patients without histological reference standard, both readers were very confident of their diagnoses so that cardiac biopsy was not performed as this is rather invasive and with the risk of severe complications. Also, in both patients with history of cardiac sarcoma the diagnosis was later confirmed by follow-up imaging. A general limitation of integrated PET/MRI is the lack of transmission-based attenuation-correction (AC) for PET data. The segmentation-based AC that was used in the present study has been shown to result in SUV measurement errors of varying degree when compared to a reference standard based on PET/CT (*16*). However, larger differences were primarily found in bone lesions and less in soft tissue (*16*). Still, SUV values close to the diagnostic cutoff need to be handled with care and visual inspection of attenuation maps for segmentation errors seems mandatory. Finally, MRI offers many more techniques for tissue differentiation that were not integrated in our study protocol to keep the overall acquisition time within certain limits. MRI techniques like rest perfusion imaging or post-contrast T1-weighted imaging with long inversion times are often used for thrombus discrimination (*20*), while (semi-)quantitative techniques like diffusion weighted imaging, T1- and T2-mapping might further improve the diagnostic accuracy in the assessment of cardiac tumors.

CONCLUSION

Simultaneous PET/MRI with ^{18}F-FDG combines detailed morphologic tumor characterization with accurate assessment of tumor malignancy and thus seems to be a powerful tool in the diagnostic workup of cardiac tumors. However, given the already strong performance of competitive methods like PET/CT and MRI, high cost and limited availability of PET/MR scanners, simultaneous PET/MRI might be reserved for selected cases were true benefit can be expected.

REFERENCES

1. McAllister H, Fenoglio J. *Tumors Of The Cardiovascular System.* In: Hartmannn W, Cowan W (eds.): Atlas of tumor pathology. Washington, DC: Armed Forces Institute of Pathology 1978: 1-20.
2. Reynen K. Frequency of primary tumors of the heart. *Am J Cardiol.* 1996;77:107.
3. Sparrow PJ, Kurian JB, Jones TR, Sivananthan MU. MR imaging of cardiac tumors. *Radiographics.* 2005;25:1255-1276.
4. Luna A, Ribes R, Caro P, Vida J, Erasmus JJ. Evaluation of cardiac tumors with magnetic resonance imaging. *Eur Radiol.* 2005;15:1446-1455.
5. Hoey ET, Mankad K, Puppala S, Gopalan D, Sivananthan MU. MRI and CT appearances of cardiac tumours in adults. *Clin Radiol.* 2009;64:1214-1230.
6. Araoz PA, Mulvagh SL, Tazelaar HD, Julsrud PR, Breen JF. CT and MR imaging of benign primary cardiac neoplasms with echocardiographic correlation. *Radiographics.* 2000;20:1303-1319.
7. Wintersperger BJ, Becker CR, Gulbins H, et al. Tumors of the cardiac valves: imaging findings in magnetic resonance imaging, electron beam computed tomography, and echocardiography. *Eur Radiol.* 2000;10:443-449.
8. Krombach GA, Spuentrup E, Buecker A, et al. [Heart tumors: magnetic resonance imaging and multislice spiral CT]. *Rofo.* 2005;177:1205-1218.
9. Hoffmann U, Globits S, Schima W, et al. Usefulness of magnetic resonance imaging of cardiac and paracardiac masses. *Am J Cardiol.* 2003;92:890-895.
10. Rahbar K, Seifarth H, Schäfers M, et al. Differentiation of malignant and benign cardiac tumors using 18F-FDG PET/CT. *J Nucl Med.* 2012;53:856-863.

11. Beiderwellen K, Gomez B, Buchbender C, et al. Depiction and characterization of liver lesions in whole body [¹□F]-FDG PET/MRI. *Eur J Radiol.* 2013;82:e669-675.
12. Wetter A, Lipponer C, Nensa F, et al. Simultaneous 18F choline positron emission tomography/magnetic resonance imaging of the prostate: initial results. *Invest Radiol.* 2013;48:256-262.
13. Grueneisen J, Beiderwellen K, Heusch P, et al. Simultaneous positron emission tomography/magnetic resonance imaging for whole-body staging in patients with recurrent gynecological malignancies of the pelvis: a comparison to whole-body magnetic resonance imaging alone. *Invest Radiol.* 2014. July 9, 2014 [Epub ahead of print].
14. Nensa F, Beiderwellen K, Heusch P, Wetter A. Clinical applications of PET/MR: current status and future perspectives. *Diagn Interv Radiol.* 2014;
15. Delso G, Fürst S, Jakoby B, et al. Performance measurements of the Siemens mMR integrated whole-body PET/MR scanner. *J Nucl Med.* 2011;52:1914-1922.
16. Martinez-Möller A, Souvatzoglou M, Delso G, et al. Tissue classification as a potential approach for attenuation correction in whole-body PET/MRI: evaluation with PET/CT data. *J Nucl Med.* 2009;50:520-526.
17. Semelka RC, Shoenut JP, Wilson ME, Pellech AE, Patton JN. Cardiac masses: signal intensity features on spin-echo, gradient-echo, gadolinium-enhanced spin-echo, and TurboFLASH images. *J Magn Reson Imaging.* 1992;2:415-420.
18. Hoffmann U, Globits S, Frank H. Cardiac and paracardiac masses. Current opinion on diagnostic evaluation by magnetic resonance imaging. *Eur Heart J.* 1998;19:553-563.

19. Nensa F, Poeppel TD, Beiderwellen K, et al. Hybrid PET/MR imaging of the heart: feasibility and initial results. *Radiology.* 2013;268:366-373.
20. Barkhausen J, Hunold P, Eggebrecht H, et al. Detection and characterization of intracardiac thrombi on MR imaging. *AJR Am J Roentgenol*. 2002;179:1539-1544.

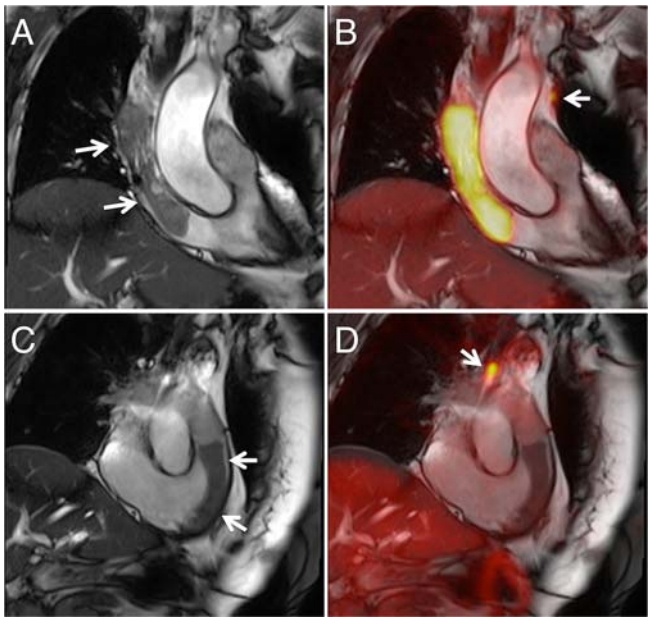

Figure 1. The first row (A and B) displays images of a patient with a history of breast cancer (Table 1, Patient 1), the second row (C and D) images of patient with anal cancer (Table 1, Patient 18). In both patients large intracavitary masses were initially found in echocardiography. The left column (A and C; arrows) shows SSFP images of large tubular masses in the superior vena cava and the right atrium (A) and in the right ventricular outflow tract (C). The right column (B and D) shows fusion images of SSFP and PET images clearly demonstrating malignancy in the patient with breast cancer (B) and a benign mass in the patient with anal cancer (D). However, closer inspection of the PET images revealed mediastinal lymph node metastases in both patients (B and D; arrows).

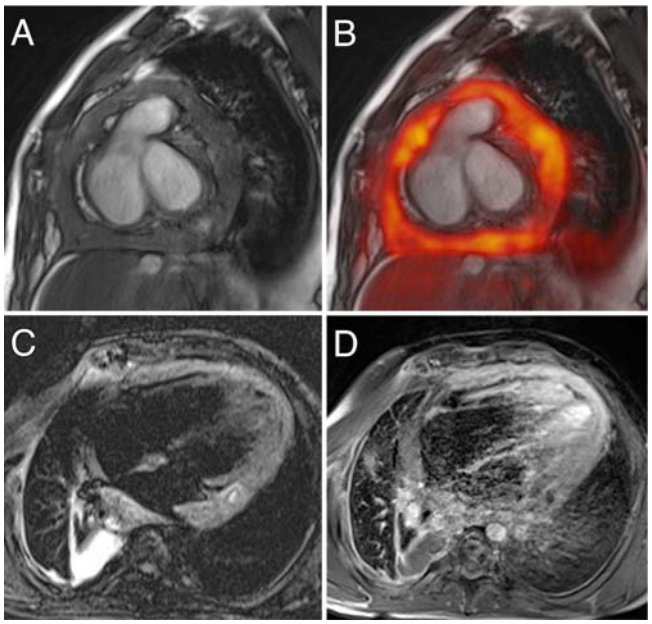

Figure 2. SSFP image (A) of a patient with local relapse of cardiac Ewings's sarcoma (Table 1, Patient 5) showing massive pericardial infiltration with intense FDG uptake (fusion B, SUV_{max} 14.6). T2-weighted images demonstrated hyperintensity of the tumor masses (C) and post-contrast T1-weighted images showed significant contrast enhancement (D).

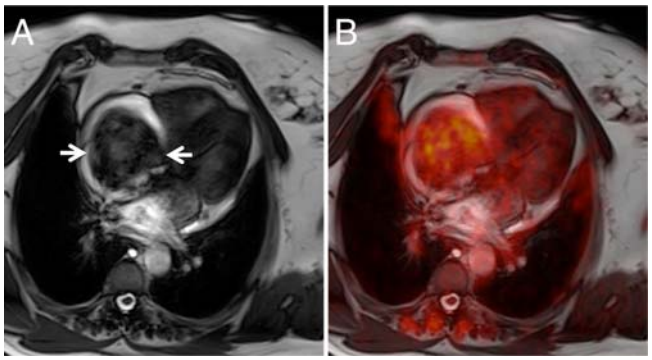

Figure 3. The left panel shows an SSFP image of large intracavitary tumor in the right atrium (A; arrows) causing dyspnea and thoracic pain (Table 1, Patient 13). The PET images (fusion B) demonstrated a mediocre FDG uptake in the tumor (SUV_{max} 3.8). Imaging diagnosis of myxoma was later confirmed by histopathology.

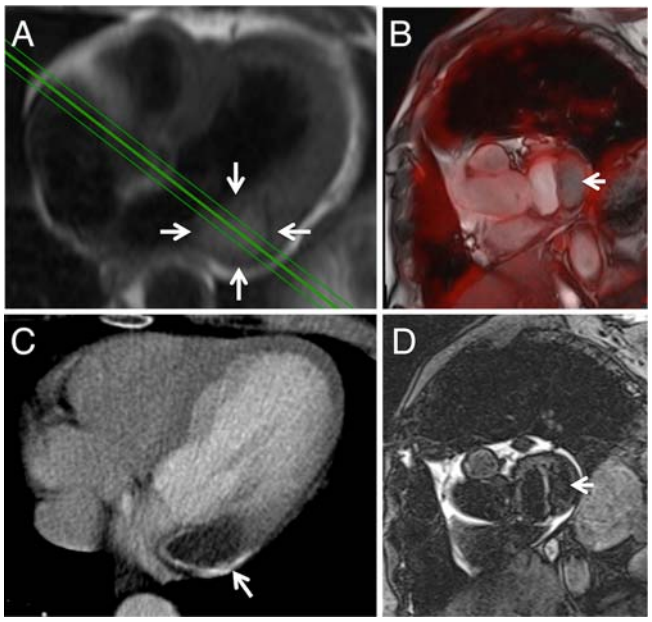

Figure 4. Axial HASTE image (A; arrows) of a lesion in the basolateral myocardial wall adjacent to the mitral valve. The lesion did not show any significant FDG uptake (fusion B; arrow). The lesion also showed calcifications on a CT scan (C; arrow) and was diagnosed as caseous calcification of the mitral annulus (Table 1, Patient 17). The lesion was hypointense on T2-weighted images (D; arrow).

TABLE 1. Patient Characteristics#

#

No	Age (y)	Sex	Location	Size [ml]	SUV_{max}	T1w	T2w	CE	Cine-MRI	PE	MRI Diagnosis	Diagnosis	Other Findings	Related Information
1	70	F	SVC and RA (intracavity)	33.2	9.6	—	↑	+	Benign		Malignant	Metastasis (Breast-Cancer)	Mediastinal lymph node metastases	Breast-Cancer (1988)
2	83	F	Pericardial masses	184.8	20.7	↑	↑	+	Malignant	+	Malignant	Metastases (Thymic carcinoma)		
3	39	F	LV (septum and lateral wall)	23.1	5.2	↑	↑	+	Malignant		Malignant	Metastases (Angiosarcoma)		Angiosarcoma of the right limb
4	57	F	LA (intracavity)	29.2	13.6	—	↑	+	Malignant	+	Malignant	Non Small Cell Lung Cancer		Infiltration via pulmonary vein
5	20	M	Massive pericardial infiltration	499	14.6	—	↑	+	Malignant	+	Malignant	Ewing's sarcoma (local relapse)		Cardiac Ewing's sarcoma, Local restaging after surgery
6	36	F	RA and RV (lateral wall)	55.3	21.3	—	↑	+	Malignant	+	Malignant	Angiosarcoma (local relapse)	Pulmonary metastases	Cardiac angiosarcoma, local Local restaging after surgery
7	78	M	RA and RV (lateral wall)	155.9	7.6	—	↑	+	Malignant	+	Malignant	Burkitt's lymphoma	Pleural effusion	
8	66	F	RA (lateral wall)	18.1	2.2	↑	↑	+	Malignant		Malignant	Scar tissue after surgery of cardiac angiosarcoma		local restaging, no histology (confirmed via follow-up MRI after 4 month)
9	21	M	RA and IVC (wall)	5.23	5.2	—	—		Benign		Benign	Patch tissue after surgery of cardiac fibrosarcoma	Thoracic wall metastasis	local restaging, no histology (confirmed via follow-up MRI after 3 month)
10	65	F	RA (intracavity, attached to septum)	5.8	1.2	—	—	+	Benign		Benign	Myxoma		
11	50	F	LA (intracavity, attached to septum)	3	1.8	—	↑	+	Benign		Benign	Myxoma		
12	83	F	LA (intracavity, attached to septum)	12.8	3	↑	↑	+	Benign		Benign	Myxoma		
13	63	F	RA (intracavity)	84.5	3.8	↑	↓	+	Benign		Benign	Myxoma		
14	67	F	Aortal valve (intracavity)	0.5	2.1	—	—	+	Benign		Benign	Fibroelastoma	Severe heart failure	
15	50	M	LA (attached to mitral valve)	36.5	1.6	—	↓		Benign		Benign	CCMA		No histology
16	45	M	LA (attached to mitral valve)	6.1	2.8	↑	—	+	Benign	+	Benign	CCMA	LV hypertrophy	No histology
17	72	M	LA (attached to mitral valve)	21.5	1.5	↑	—		Benign		Benign	CCMA		No histology
18	57	F	RVOT	10.3	1.3	—	↑		Benign	+	Benign	Thrombus	Mediastinal lymph node metastases	Anal-Carcinoma
19	78	F	LA (intracavity, attached superior wall)	22.1	1	—	↑		Benign		Benign	Thrombus		
20	50	M	Ascending aorta (attached to wall, floating)	0.6	2	↑	↑		Benign		Benign	Thrombus		

LA = left atrium; LV = left ventricle; RA = right atrium; RV = right ventricle; RVOT = right ventricular outflow tract; SVC = superior vena cava; IVC = inferior vena cava; CE = contrast enhancement; PE = pericardial effusion; CCMA = caseous calcification of mitral annulus; ↑ = hyperintense; ↓ = hypointense; — = isointense; + = feature present

#

TABLE 2. Diagnostic Performance of PET and MR Features

Feature	Sensitivity [%]	Specificity [%]	PPV [%]	NPV [%]
SUV_{max} (Cutoff: ≥ 5.2, optimal)	100	92	88	100
SUV_{max} (Cutoff: ≥ 3.5, see Rhabar et al.)	100	85	78	100
Tumor Volume (Cutoff: ≥ 23.1 ml, optimal)	100	85	78	100
Pericardial Effusion	71	85	71	85
Cine SSFP Morphology	86	92	86	92
T1w Hyperintensity	29	54	25	58
T2w Hyperintensity	100	54	54	100
Contrast-Enhancement	100	46	50	100
MRI Overall	100	92	88	100
MRI Overall & SUV_{max} (Cutoff: ≥ 5.2, optimal)	100	100	100	100

PPV = positive predictive value; NPV = negative predictive value; & = Boolean ‘AND’ combination